GA–A27767

EXPERIMENTAL AND SIMULATION TESTING OF PHYSICS-MODEL-BASED SAFETY FACTOR PROFILE AND INTERNAL ENERGY FEEDBACK CONTROLLERS IN DIII-D ADVANCED TOKAMAK SCENARIOS

by

J.E. BARTON, M.D. BOYER, W. SHI, W.P. WEHNER, E. SCHUSTER,
J.R. FERRON, M.L. WALKER, D.A. HUMPHREYS, T.C. LUCE, F. TURCO,
R.D. JOHNSON, and B.G. PENAFLOR

APRIL 2014

GENERAL ATOMICS

DISCLAIMER

GA–A27767

EXPERIMENTAL AND SIMULATION TESTING OF PHYSICS-MODEL-BASED SAFETY FACTOR PROFILE AND INTERNAL ENERGY FEEDBACK CONTROLLERS IN DIII-D ADVANCED TOKAMAK SCENARIOS

by
J.E. BARTON,* M.D. BOYER,* W. SHI,* W.P. WEHNER,* E. SCHUSTER,*
J.R. FERRON, M.L. WALKER, D.A. HUMPHREYS, T.C. LUCE, F. TURCO,†
R.D. JOHNSON, and B.G. PENAFLOR

This is a preprint of a paper to be presented at the 19th World Congress IFAC'14, August 24–29, 2014 Cape Town, South Africa, and published in the *Proceedings*.

*Lehigh University, Bethlehem, Pennsylvania.
†Columbia University, New York, New York.

Work supported by in part by
the U.S. Department of Energy
under DE-FC02-04ER54698 and DE-FG02-04ER54761

GENERAL ATOMICS PROJECT 30200
APRIL 2014

GENERAL ATOMICS

Experimental and Simulation Testing of Physics-model-based Safety Factor Profile and Internal Energy Feedback Controllers in DIII-D Advanced Tokamak Scenarios ⋆

Justin E. Barton * **Mark D. Boyer** * **Wenyu Shi** *
William P. Wehner * **Eugenio Schuster** * **John R. Ferron** **
Michael L. Walker ** **David A. Humphreys** ** **Tim C. Luce** **
Francesca Turco *** **Robert D. Johnson** ** **Ben G. Penaflor** **

* *Lehigh University, Bethlehem, PA 18015, USA.*
** *General Atomics, San Diego, CA 92121, USA.*
*** *Columbia University, New York, NY 10027, USA.*

Abstract: Active closed-loop control of the plasma safety factor profile (q-profile) and internal energy dynamics in nuclear fusion tokamak devices has the potential to significantly impact the success of the ITER project. These plasma properties are related to both the stability and performance of a given plasma operating scenario. In this work, we develop integrated feedback control algorithms to control the q-profile and internal energy dynamics in DIII-D advanced tokamak (high performance) scenarios. The feedback controllers are synthesized by embedding a nonlinear, physics-based, control-oriented partial differential equation model of the plasma dynamics into the control design and to be robust to uncertainties in the plasma electron density, electron temperature, and plasma resistivity profiles. The auxiliary heating and current-drive system and the total plasma current are the actuators utilized by the feedback controllers to control the plasma dynamics. Finally, the feedback controllers are tested both through simulations based on the physics-based model and experimentally in the DIII-D tokamak.

1. INTRODUCTION

One of the most promising magnetic confinement devices utilized to create the conditions necessary for thermonuclear fusion to occur is the tokamak (Wesson (2004)). In a tokamak, externally applied magnetic fields are used to confine a reactant gas, which is in the plasma state, in a fixed volume by exploiting the plasma's ability to conduct electrical current. Two properties that are often employed to define a plasma operating scenario are the safety factor profile (q-profile), which is related to the plasma stability and performance, and the normalized plasma beta (β_N), which is a measure of the confinement efficiency of the plasma magnetic configuration (Wesson (2004)). Therefore, closed-loop q-profile and plasma β_N control has the potential to significantly impact the success of the ITER project, which is the next phase of tokamak development.

Closed-loop q-profile control was recently demonstrated in low confinement (L-mode) (Wesson (2004)) scenarios at the DIII-D tokamak (Barton et al. (2012); Boyer et al. (2013, 2014)). The utilized controllers were synthesized by embedding a nonlinear, physics-based, partial differential equation (PDE) model of the plasma dynamics into the control design. In this work, we extend this control philosophy to develop feedback algorithms for integrated q-profile and plasma β_N control in DIII-D high confinement (H-mode) advanced tokamak scenarios (Wesson (2004)).

⋆ This work was supported by the U.S. Department of Energy (DE-SC0001334, DE-SC0010661 and DE-FC02-04ER54698). E-mail contact of first author: justin.barton@lehigh.edu

The coupling between the plasma magnetic and kinetic states increases in H-mode scenarios (characterized by transport barriers (Wesson (2004)) just inside the plasma boundary) through the increase of the noninductive bootstrap current (a self-generated current) (Peeters (2000)). In Barton et al. (2013), a general control-oriented physics-based modeling approach has been developed to convert the first-principles physics model that describes the plasma poloidal magnetic flux profile evolution (related to the q-profile) into a form suitable for control design, with emphasis on H-mode scenarios. The plasma internal energy (related to the plasma β_N) is modeled by a volume-averaged plasma energy balance equation. Feedback algorithms to control the q-profile and plasma β_N evolutions in H-mode scenarios in DIII-D are developed by embedding these physics-based models of the plasma dynamics into the control synthesis. Additionally, the controllers are designed to be robust to uncertainties in the plasma electron density, electron temperature, and plasma resistivity profiles. The actuators used to control the plasma dynamics are the auxiliary heating and current-drive (H&CD) system and total plasma current. Finally, the controllers are tested both through simulations based on the physics-based models of the plasma dynamics and experimentally in DIII-D.

2. PLASMA STATE EVOLUTION MODELS

A well confined tokamak plasma equilibrium is characterized by the formation of nested surfaces of constant poloidal magnetic flux. In this work, the magnetic flux

surfaces are indexed by their mean effective minor radius, ρ, i.e., $\Phi(\hat{\rho}) = \pi B_{\phi,0}\rho^2$, where Φ is the toroidal magnetic flux and $B_{\phi,0}$ is the vacuum toroidal magnetic field at the geometric major radius R_0 of the tokamak. The normalized effective minor radius is defined as $\hat{\rho} = \rho/\rho_b$, where ρ_b is the mean effective minor radius of the last closed magnetic flux surface.

The q-profile is related to the spatial gradient of the poloidal magnetic flux Ψ and is defined as

$$q(\hat{\rho},t) = -\frac{d\Phi}{d\Psi} = -\frac{d\Phi}{2\pi d\psi} = -\frac{B_{\phi,0}\rho_b^2\hat{\rho}}{\partial\psi/\partial\hat{\rho}}, \quad (1)$$

where t is the time and ψ is the poloidal stream function, which is closely related to the poloidal flux ($\Psi = 2\pi\psi$). The plasma β_N is related to the volume-averaged plasma internal energy E and is defined as

$$\beta_N = \beta_t[\%]\frac{aB_{\phi,0}}{I_p} \quad \beta_t = \frac{\langle p\rangle_V}{B_{\phi,0}^2/(2\mu_0)} = \frac{(2/3)(E/V_p)}{B_{\phi,0}^2/(2\mu_0)}, \quad (2)$$

where β_t is the toroidal plasma beta (Wesson (2004)), a is the plasma minor radius, I_p is the total plasma current (evaluated in units of MA), p is the plasma kinetic pressure, $\langle\cdot\rangle_V$ denotes the volume-average operation $1/V_p\int_V(\cdot)dV$, V is the volume enclosed by a magnetic flux surface, V_p is the total plasma volume, and μ_0 is the vacuum magnetic permeability. Therefore, the q-profile and plasma β_N can be controlled if we are able to control the poloidal flux gradient profile, which we define as

$$\theta(\hat{\rho},t) \equiv \partial\psi/\partial\hat{\rho}(\hat{\rho},t), \quad (3)$$

and the plasma internal energy, assuming the magnetic geometry is time invariant and the system is controllable.

We begin by converting the physics model that describes the poloidal magnetic flux profile evolution in the tokamak (the magnetic diffusion equation (Hinton and Hazeltine (1976))) into a form suitable for control design. The auxiliary H&CD actuators on DIII-D considered in this work are 1 effective electron cyclotron (gyrotron) microwave launcher and 6 co-current neutral beam injectors (NBI), which are referred to by the names [30L/R,150L/R,330L/R], where L and R denote left and right NBI lines, respectively. In the H&CD scheme considered, the gyrotrons inject power into the plasma in the spatial region $\hat{\rho} \in [0.3, 0.7]$, the 30L/R and 330L/R neutral beams inject power into the plasma with a deposition profile that is peaked at the magnetic axis (referred to as on-axis NBI), and the 150L/R neutral beams inject power into the plasma with a deposition profile that is peaked away from the magnetic axis in the spatial region $\hat{\rho} \in [0.3, 0.5]$ (referred to as off-axis NBI) (Barton et al. (2013)). The magnetic axis is the limiting magnetic flux surface at the center of the plasma. Simplified physics-based models of the noninductive current-drives are discussed in Barton et al. (2013). The auxiliary gyrotron and neutral beam current-drives are proportional to the current-drive efficiencies T_e/n_e and $\sqrt{T_e}/n_e$, respectively, where T_e and n_e are the electron temperature and density profiles, respectively. The bootstrap current (j_{bs}) is proportional to the inverse of the poloidal flux gradient profile multiplied by the kinetic plasma profile gradients, i.e., $j_{bs} \propto (\theta)^{-1}[n_e\frac{\partial T_e}{\partial\hat{\rho}} + T_e\frac{\partial n_e}{\partial\hat{\rho}}]$.

We define ranges in which the electron density and temperature profiles are expected to be in typical DIII-D advanced scenarios, which are shown in Figs. 1(a-b). We model these parameters as a nominal profile plus a bounded uncertain profile, i.e.,

$$n_e(\hat{\rho},t) = n_e^{nom}(\hat{\rho}) + n_e^{unc}(\hat{\rho})\delta_{n_e}(t), \quad (4)$$
$$T_e(\hat{\rho},t) = T_e^{nom}(\hat{\rho}) + T_e^{unc}(\hat{\rho})\delta_{T_e}(t), \quad (5)$$

where the nominal (n_e^{nom}, T_e^{nom}) and uncertain profiles (n_e^{unc}, T_e^{unc}) are defined in terms of the maximum and minimum profiles shown in Figs. 1(a-b), with $|\delta_{T_e}| \le 1$ and $|\delta_{n_e}| \le 1$. The plasma resistivity is inversely related to the electron temperature (minimum resistivity is defined by the maximum electron temperature), and the resistivity range is shown in Fig. 1(c). Additionally, the parameters $\sqrt{T_e}$ and $1/n_e$ are related to the electron temperature and density, respectively. These parameters are modeled as

$$\eta(\hat{\rho},t) = \eta^{nom}(\hat{\rho}) + \eta^{unc}(\hat{\rho})\delta_{T_e}(t), \quad (6)$$
$$\sqrt{T_e(\hat{\rho},t)} = T_e^{nom'}(\hat{\rho}) + T_e^{unc'}(\hat{\rho})\delta_{T_e}(t), \quad (7)$$
$$1/n_e(\hat{\rho},t) = n_e^{nom'}(\hat{\rho}) + n_e^{unc'}(\hat{\rho})\delta_{n_e}(t), \quad (8)$$

where the nominal (η^{nom}, $T_e^{nom'}$, $n_e^{nom'}$) and uncertain (η^{unc}, $T_e^{unc'}$, $n_e^{unc'}$) profiles are defined in terms of the maximum and minimum profiles shown in Fig. 1.

By combining the magnetic diffusion equation (Hinton and Hazeltine (1976)) with the noninductive current-drive models (Barton et al. (2013)) and the models (4)-(8), the PDE governing the evolution of θ is given by

$$\begin{aligned}\frac{\partial\theta}{\partial t} &= [q_1(\hat{\rho}) + q_4(\hat{\rho})\delta_{T_e}]\frac{\partial^2\theta}{\partial\hat{\rho}^2} + [q_2(\hat{\rho}) + q_5(\hat{\rho})\delta_{T_e}]\frac{\partial\theta}{\partial\hat{\rho}}\\ &+ [q_3(\hat{\rho}) + q_6(\hat{\rho})\delta_{T_e}]\theta + \sum_i \big[g_i'(\hat{\rho}) + h_i'(\hat{\rho})\delta_{n_e}\\ &+k_i'(\hat{\rho})\delta_{T_e} + l_i'(\hat{\rho})\delta_{T_e}\delta_{n_e} + m_i'(\hat{\rho})\delta_{T_e}^2\\ &+p_i'(\hat{\rho})\delta_{T_e}^2\delta_{n_e}\big]P_i(t) - \big[g_{bs}(\hat{\rho}) + h_{bs}(\hat{\rho})\delta_{n_e} + k_{bs}(\hat{\rho})\delta_{T_e}\\ &+l_{bs}(\hat{\rho})\delta_{T_e}\delta_{n_e} + m_{bs}(\hat{\rho})\delta_{T_e}^2 + p_{bs}(\hat{\rho})\delta_{T_e}^2\delta_{n_e}\big]\left(\frac{1}{\theta}\right)^2\frac{\partial\theta}{\partial\hat{\rho}}\\ &+\big[g_{bs}'(\hat{\rho}) + h_{bs}'(\hat{\rho})\delta_{n_e} + k_{bs}'(\hat{\rho})\delta_{T_e} + l_{bs}'(\hat{\rho})\delta_{T_e}\delta_{n_e}\\ &+m_{bs}'(\hat{\rho})\delta_{T_e}^2 + p_{bs}'(\hat{\rho})\delta_{T_e}^2\delta_{n_e}\big]\left(\frac{1}{\theta}\right), \end{aligned} \quad (9)$$

with boundary conditions

$$\theta(0,t) = 0 \qquad \theta(1,t) = -k_{I_p}I_p(t), \quad (10)$$

where $i \in \{ec_{tot}, nbi_{30L/R}, nbi_{150L/R}, nbi_{330L/R}\}$, the parameters $q_k(\hat{\rho})$, for $k = 1,\ldots,6$, $g_i(\hat{\rho})$, $h_i(\hat{\rho})$, $k_i(\hat{\rho})$, $l_i(\hat{\rho})$, $m_i(\hat{\rho})$, $p_i(\hat{\rho})$, $g_{bs}(\hat{\rho})$, $h_{bs}(\hat{\rho})$, $k_{bs}(\hat{\rho})$, $l_{bs}(\hat{\rho})$, $m_{bs}(\hat{\rho})$, $p_{bs}(\hat{\rho})$ are functions of space, $(\cdot)' = d/d\hat{\rho}$, k_{I_p} is a constant, and $P_i(t)$ is the total gyrotron launcher power and the individual neutral beam injection powers, respectively. The volume-averaged plasma energy balance is given by

$$\frac{dE}{dt} = -\frac{E}{\tau_E(t)} + P_{aux}(t) = -\frac{E}{\tau_E(t)} + \sum_i P_i(t), \quad (11)$$

where $\tau_E(t)$ is the global energy confinement time, P_{aux} is the total auxiliary heating power, and we have neglected the ohmic and radiated power as they are typically small compared to P_{aux} in the scenarios considered. The energy confinement time scaling used in this work is the IPB98(y,2) scaling law (ITER Physics Basis (1999)).

3. SPATIAL DISCRETIZATION OF PDE MODEL

We spatially discretize the governing PDE (9) by employing a finite difference method, where the spatial domain of

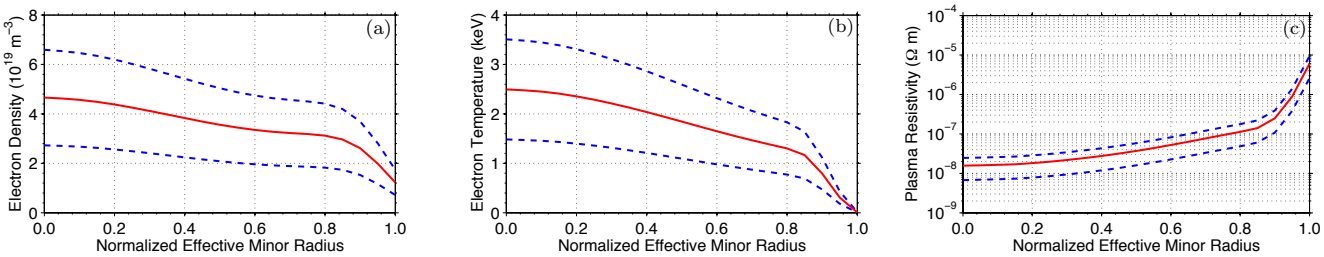

Fig. 1. Plasma parameter uncertainty ranges: (a) electron density, (b) electron temperature, and (c) plasma resistivity. Note: nominal values (solid) and minimum/maximum values (dash).

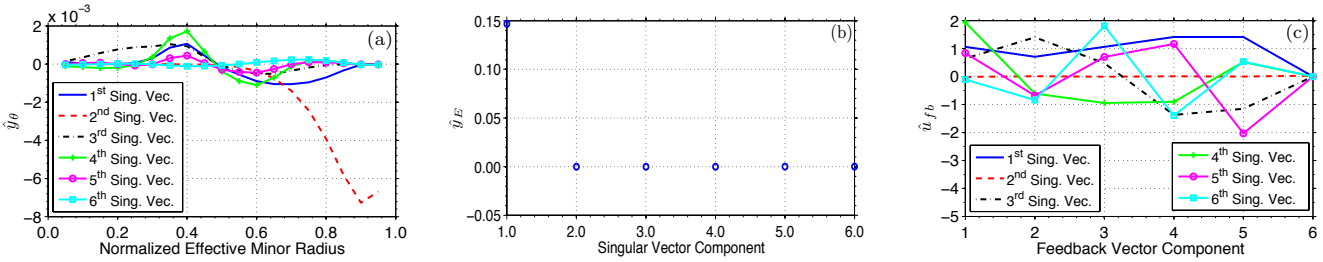

Fig. 2. Relevant control channels: (a-b) output and (c) input. The decoupled output is defined as $\hat{y} = [\hat{y}_\theta, \hat{y}_E]$ where $\hat{y}_\theta$ are the system outputs associated with the magnetic states and $\hat{y}_E$ is the system output associated with the kinetic states. The feedback vector components are $u_{fb} = [P_{ec_{tot}}, P_{nbi_{150L/R}}, P_{nbi_{330L/R}}, I_p]$ where $u_{fb} = 0$ for $P_{nbi_{30L/R}}$.

interest, $\hat{\rho} \in [0,1]$, is represented as m_θ nodes, to obtain a model suitable for tracking control design. After spatially discretizing (9) and taking into account the boundary conditions (10), we obtain a nonlinear, finite dimensional, ordinary differential equation model defined by

$$\dot{\hat{\theta}} = f_\theta(\hat{\theta}, u, \delta),$$

where $\hat{\theta} = [\theta_2, \ldots, \theta_{m_\theta - 1}]^T \in \mathbb{R}^{n_\theta}$ is the magnetic state vector, θ_i, for $i = 2, \ldots, m_\theta - 1$, is the value of θ at the i-th node, $u = [P_{ec_{tot}}, P_{nbi_{30L/R}}, P_{nbi_{150L/R}}, P_{nbi_{330L/R}}, I_p]^T \in \mathbb{R}^8$ is the control input vector, the uncertain parameter vector is $\delta = \left[\delta_{T_e}, \delta_{n_e}, \delta_{T_e}\delta_{n_e}, \delta^2_{T_e}, \delta^2_{T_e}\delta_{n_e}\right]^T \in \mathbb{R}^5$, $f_\theta \in \mathbb{R}^{n_\theta}$ is a nonlinear function of the plasma magnetic states, control inputs, and uncertain parameters, and $n_\theta = m_\theta - 2$. By defining the plasma state vector as $x = [\hat{\theta}, E] \in \mathbb{R}^{(n_\theta+1)}$, we can write the magnetic and kinetic state dynamics as

$$\dot{x} = \begin{bmatrix} f_\theta(\hat{\theta}, u, \delta) \\ -\dfrac{E}{\tau_E(t)} + \displaystyle\sum_{i=1}^{7} u_i \end{bmatrix} = F_{\theta,E}(x, u, \delta) \in \mathbb{R}^{(n_\theta+1)}. \quad (12)$$

Linearizing (12) with respect to the state and control input around a nominal equilibrium point $(x_{eq}, u_{eq}, 0)$, we obtain a linear time-invariant (LTI) model given by

$$\dot{\tilde{x}} = A\tilde{x} + Bu_{fb} + d \qquad y = C\tilde{x} + Du_{fb}, \quad (13)$$

with

$$A = A_0 + \sum_{m=1}^{5} \delta_m A_m \qquad B = B_0 + \sum_{m=1}^{5} \delta_m B_m,$$
$$C = C_0 + \sum_{m=1}^{5} \delta_m C_m \qquad D = D_0 + \sum_{m=1}^{5} \delta_m D_m, \quad (14)$$

where $\tilde{x}(t) = x(t) - x_{eq}$, $u_{fb}(t) = u(t) - u_{eq}$ is the output of the to-be-designed feedback controller, $d(t) = F_{\theta,E}(x_{eq}, u_{eq}, \delta)$, A and B are the Jacobians $\partial F_{\theta,E}/\partial x \in \mathbb{R}^{(n_\theta+1)\times(n_\theta+1)}$ and $\partial F_{\theta,E}/\partial u \in \mathbb{R}^{(n_\theta+1)\times 8}$, respectively, evaluated at (x_{eq}, u_{eq}), A_i and B_i, for $i = 0, \ldots, 5$, are the components of the matrices A and B, respectively, C_0 is an $(n_\theta+1)\times(n_\theta+1)$ identity matrix, $D_0 = 0$, and $C_j = 0$ and $D_j = 0$, for $j = 1, \ldots, 5$.

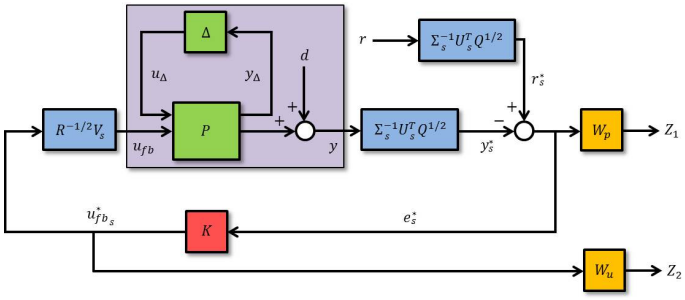

Fig. 3. Schematic of feedback control problem formulation.

4. RELEVANT CONTROL CHANNELS

In order to acquire diagnostic data that is needed by the real-time EFIT (rtEFIT) equilibrium reconstruction code (Ferron et al. (1998)) to reconstruct the plasma q-profile for feedback control, the 30L/R neutral beam powers need to be constant, and we do not utilize them for feedback control, i.e., $u_{fb} = 0$ for $P_{nbi_{30L/R}}$. As a result, we have six actuators to utilize in feedback, which implies we can independently control at most six linear combinations of the system output. To identify the relevant control channels, we employ a singular value decomposition (SVD) of the nominal state-space system $y = G_0(s)u_{fb} = (C_0(sI_{n_\theta} - A_0)^{-1}B_0 + D_0)u_{fb}$ at a particular frequency.

The real approximation of the nominal input-output relation at a particular frequency $j\omega_{dc}$ is expressed as

$$\hat{y} = \hat{G}_0 \hat{u}_{fb}, \quad (15)$$

where $\hat{y}$ denotes the decoupled/relevant output, $\hat{u}_{fb}$ denotes the decoupled/relevant input, and $\hat{G}_0$ denotes the real approximation of the complex matrix $G_0(j\omega_{dc})$ (Skogestad and Postlethwaite (2005)). By selecting the frequency as $\omega_{dc} = 25$ rad/sec., the total plasma current

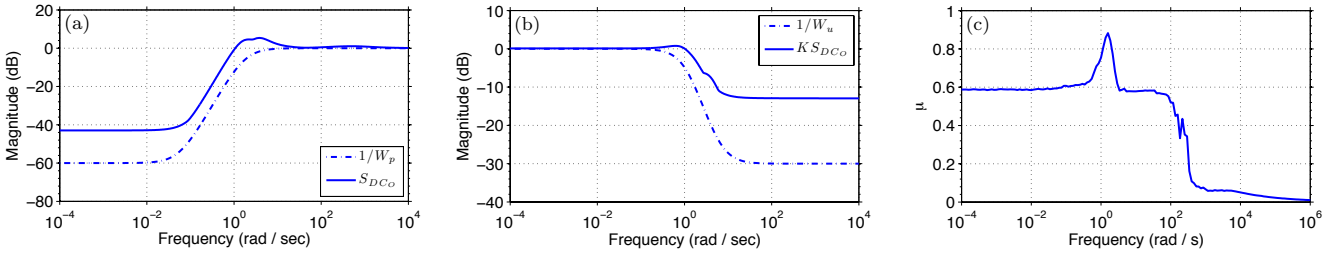

Fig. 4. Maximum singular values: (a) $1/W_p$ and S_{DC_o} and (b) $1/W_u$ and KS_{DC_o} and (c) $\mu(N_{11}(j\omega))$ versus frequency. The closed-loop robust stability condition is defined as $\mu(N_{11}(j\omega)) < 1$, $\forall\omega$ (Skogestad and Postlethwaite (2005)).

(I_p) is exclusively utilized to control the q-profile near the plasma boundary (2nd singular vector in Figs. 2(a) and 2(c)). Additionally, to weight the relative tracking performance and control effort, we introduce the positive definite weighting matrices $Q \in \mathbb{R}^{(n_\theta+1)\times(n_\theta+1)}$ and $R \in \mathbb{R}^{6\times6}$. We next define the economy size SVD of the weighted matrix $\tilde{G}_0$ as $\tilde{G}_0 = Q^{1/2}\hat{G}_0R^{-1/2} = U\Sigma V^T$, where $\Sigma = \text{diag}(\sigma_1, \sigma_2, \ldots, \sigma_6) \in \mathbb{R}^{6\times6}$ is a diagonal matrix of singular values and $U \in \mathbb{R}^{(n_\theta+1)\times6}$ and $V \in \mathbb{R}^{6\times6}$ are matrices that possess the following properties $V^TV = VV^T = I, U^TU = I$, where I is a 6×6 identity matrix, and $(\cdot)^T$ denotes the matrix transpose. The relevant control channels are then obtained from the input-output relation

$$\hat{y} = Q^{-1/2}\tilde{G}_0R^{1/2}\hat{u}_{fb} = Q^{-1/2}U\Sigma V^TR^{1/2}\hat{u}_{fb}$$

and are shown in Fig. 2. We note that some of the singular values σ_i may have a small magnitude relative to the others and may be chosen to be neglected in the control synthesis. Quantities that are associated with the significant singular values (the ones retained in the control design) are denoted by a subscript s for the remainder of this paper, i.e., $(\cdot)_s$. More details regarding this technique can be found in Barton et al. (2012); Ambrosino et al. (2007).

5. FEEDBACK CONTROLLER SYNTHESIS

By exploiting the structure of the of the state matrices in (14), the feedback system (13) can be written in the conventional $P-\Delta$ control framework (shown in the light purple box in Fig. 3), where P is the generalized plant and $\Delta = \text{diag}\{\delta_{T_e}, \delta_{n_e}\}$ is a structured uncertainty matrix, by employing the method outlined in Packard (1988). The system input-output equations in this framework are

$$y_\Delta = P_{11}u_\Delta + P_{12}u_{fb} \qquad y = P_{21}u_\Delta + P_{22}u_{fb} + d, \quad (16)$$

where P_{11}, P_{12}, P_{21}, and P_{22} are the component transfer functions of the generalized plant P that are related to the system outputs (y_Δ, y) and inputs (u_Δ, u_{fb}), respectively.

It is desired that the output y be able to track a reference value r, therefore, we define the tracking error as $e = r - y$. The feedback control problem is formulated as shown in Fig. 3, where K is the feedback controller, $Z_1 = W_pe_s^*$, $Z_2 = W_uu_{fb_s}^*$, and W_p and W_u are frequency dependent weight functions used to optimize the closed-loop performance. The nominal performance condition of the closed-loop system is expressed as

$$\begin{bmatrix} Z_1 \\ Z_2 \end{bmatrix} = \begin{bmatrix} W_pS_{DC_O} & -W_pS_{DC_O} \\ W_uKS_{DC_O} & -W_uKS_{DC_O} \end{bmatrix} \begin{bmatrix} r_s^* \\ d_s^* \end{bmatrix} \triangleq T_{zw} \begin{bmatrix} r_s^* \\ d_s^* \end{bmatrix},$$

where $S_{DC_O} = (I+\Sigma_s^{-1}U_s^TQ^{1/2}P_{22}R^{-1/2}V_sK)^{-1}$, and the control problem is formulated as

$$\min_K \left|\left|T_{zw}\right|\right|_\infty, \quad \forall\omega. \qquad (17)$$

The feedback controller written in terms of the tracking error e and control input u_{fb} is expressed as

$$\begin{aligned} \dot{x}_{fb} &= A_{fb}x_{fb} + B_{fb}\Sigma_s^{-1}U_s^TQ^{1/2}e, \\ u_{fb} &= R^{-1/2}V_sC_{fb}x_{fb} + R^{-1/2}V_sD_{fb}\Sigma_s^{-1}U_s^TQ^{1/2}e, \end{aligned} \quad (18)$$

where x_{fb} is the internal controller state vector and A_{fb}, B_{fb}, C_{fb}, D_{fb} are the state-space matrices of the controller K that are determined by solving (17). To analyze the performance and robust stability of the closed-loop system, the maximum singular value diagrams of the inverse of the performance weight functions and the achieved transfer functions S_{DC_O} and KS_{DC_O} are shown in Figs. 4(a-b) and a plot of the structured singular value $\mu(N_{11}(j\omega))$ versus frequency is shown in Fig. 4(c), where $N_{11} = P_{11}-P_{12}R^{-1/2}V_sKS_{DC_O}\Sigma_s^{-1}U_s^TQ^{1/2}P_{21}$ is the closed-loop transfer function between y_Δ and u_Δ in Fig. 3.

6. SIMULATION TESTING OF SAFETY FACTOR PROFILE AND PLASMA β_N CONTROLLER

In this section, the q-profile + β_N feedback controller (18) is tested through simulations based on the physics-based model of the poloidal magnetic flux profile dynamics developed in Barton et al. (2013) and the volume-averaged plasma energy balance (11) tailored to DIII-D H-mode scenarios. To ensure the closed-loop system remains well behaved in the presence of actuator magnitude saturation, the controller is augmented with an anti-windup compensator. First, a target q-profile and β_N evolution is obtained by executing a feedforward-only simulation with the control input trajectories and initial conditions $(q(\hat{\rho}, 0.5)$ and $\beta_N(0.5))$ achieved in DIII-D shot 150318. Second, a nominal q-profile and β_N evolution is obtained by executing a feedforward-only simulation with a nominal set of input trajectories and initial conditions. Finally, the ability of the algorithm to track the target evolutions is determined by executing a feedforward + feedback simulation with the nominal input trajectories and initial conditions. During the feedback-controlled simulation, the controller is inactive during the time interval $t = [0.5, 2.0]$ sec. Simulated white noise is added to both the feedforward + feedback and feedforward simulations, respectively, to approximately replicate the noise level observed in the rtEFIT measurements during DIII-D operations.

Time traces of q at various spatial locations, a time trace of the plasma β_N, and a comparison of the control inputs $(P_{off-axis} = P_{ec_{tot}} + P_{nbi_{150L}} + P_{nbi_{150R}}$ and $P_{on-axis} = P_{nbi_{330L}} + P_{nbi_{330R}})$ is shown in Fig. 5. As shown in the figures, the controller is able to drive the q-profile and plasma β_N to the target evolutions once it becomes active at 2.0 sec. during the feedback-controlled simulation. The

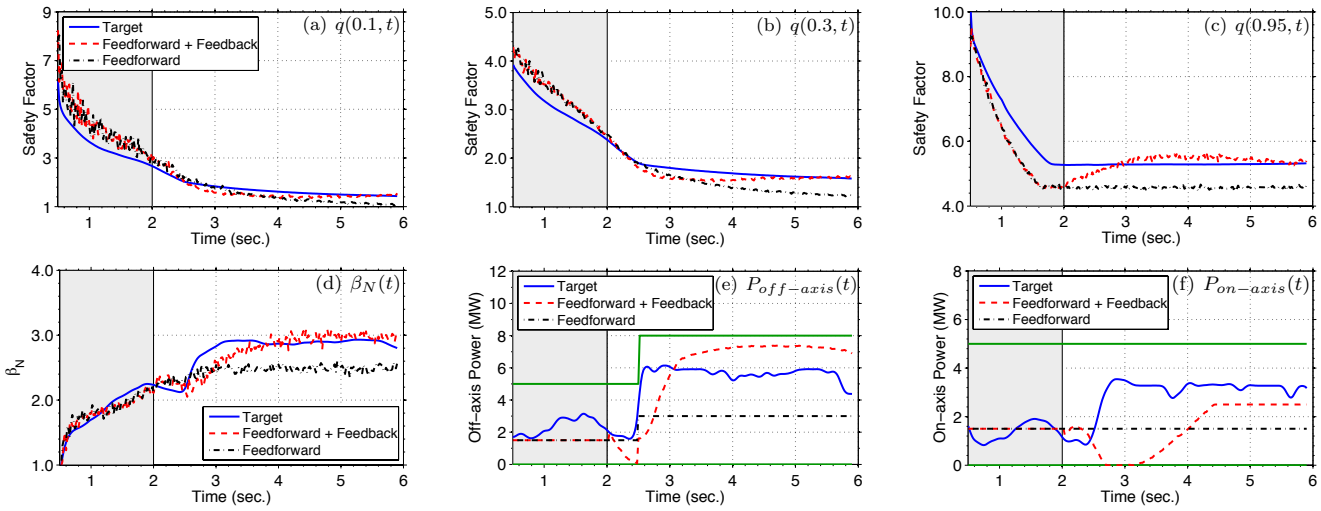

Fig. 5. Simulation testing of q-profile + β_N feedback controller: (a-c) time trace of q at various spatial locations, (d) time trace of plasma β_N, and (e-f) control actuator trajectory comparison (actuator limits in solid green). The gray-shaded region indicates when the feedback controller is inactive. Note gyrotrons become available at 2.5 sec.

local q-value is roughly inversely related to the local current density amplitude in tokamaks, i.e., a low q-profile is characterized by a high current profile and vice versa. In the feedback-controlled simulation, firstly, the controller decreases the total plasma current to eliminate the error in q near the plasma boundary. Secondly, at approximately 2.5 sec., the value of q in the plasma core evolves below the target value. In response, the controller decreases the on-axis auxiliary current-drive ($P_{nbi_{330\mathrm{L/R}}}$) and increases the off-axis auxiliary current-drive ($P_{ec_{tot}}$ and $P_{nbi_{150\mathrm{L/R}}}$) to track the target q-profile in the plasma core. Finally, in order to track the target plasma β_N while maintaining good tracking of the q-profile in the plasma core, the controller slowly increases the on-axis auxiliary heating (specifically $P_{nbi_{330\mathrm{R}}}$) beginning at approximately 3.25 sec.

7. EXPERIMENTAL TESTING OF SAFETY FACTOR PROFILE CONTROLLER IN THE DIII-D TOKAMAK

In this section, the q-profile feedback controller is experimentally tested in an H-mode scenario in DIII-D. Note that the q-profile controller is designed by removing the plasma internal energy from the system outputs in (13). It is also important to emphasize that the actuator requests generated by the controller represent the references to dedicated control loops that command the physical actuators.

In DIII-D shot 154692, the q-profile feedback controller was tested in a disturbance rejection experiment. The q-profile evolution achieved in DIII-D shot 154358 was chosen as the target. The disturbance introduced to the plasma in shot 154692 was to delay the time at which the plasma transitioned from L-mode to H-mode. This delay resulted in the inductive component of the plasma current profile diffusing in towards the plasma core at a faster rate than in the target shot. As a result, there was a significant perturbation in the initial q-profile at 0.5 sec. (low relative to the target) in the feedback-controlled experiment. Also during the feedforward + feedback shot 154692, the feedforward component of the control input was frozen after 1.6 sec. Therefore, the achieved profile regulation was obtained exclusively through feedback.

A comparison of the target and feedforward + feedback controlled q-profiles at various times, time traces of q at various spatial locations, a time trace of the plasma β_N, and a comparison of the control inputs ($P_{nbi_{off}} = P_{nbi_{150L}} + P_{nbi_{150R}}$ and $P_{nbi_{on}} = P_{nbi_{330L}} + P_{nbi_{330R}}$) is shown in Fig. 6. As shown in the figures, the controller was able to reject the effects of the initial condition error and drive the q-profile to the target evolution during the approximate time interval $t \in [0.5, 3.5]$ sec. The controller utilized the total plasma current to regulate the q-profile evolution near the plasma boundary and modulated the mix of on-and-off axis auxiliary current-drive to track the target q-profile evolution in the plasma core as shown in Figs. 6(h-i). However, even though the feedback controller requested the maximum amount of the off-axis auxiliary current-drive during the time interval $t \in [4.0, 6.0]$ sec., the q-profile in the plasma core was unable to be maintained at the target. Two factors that contributed to this were the inability of the dedicated control loops commanding the physical actuators to follow the line average electron density request and to deliver any gyrotron power (shown in Fig. 7). These factors contributed to the achieved plasma β_N being relatively far away from the target during the approximate time interval $t \in [3.0, 6.0]$ sec. (shown in Fig. 6(g)). As the plasma β_N is a measure of the confinement efficiency of a plasma equilibrium, the energy confinement time of the plasma was lower in the feedback-controlled experiment relative to the target. The reduced energy content of the plasma, along with the poor regulation of the electron density, may have contributed to a lower bootstrap current ($j_{bs} \propto (\theta)^{-1}[n_e \frac{\partial T_e}{\partial \hat{\rho}} + T_e \frac{\partial n_e}{\partial \hat{\rho}}]$) in the feedback-controlled experiment. As the bootstrap current is an off-axis noninductive source of current, a lower bootstrap current may have contributed to the inability to maintain the q-profile in the plasma core at the target during the feedback-controlled experiment.

8. CONCLUSIONS AND FUTURE WORK

Robust feedback algorithms to control the q-profile and plasma β_N evolutions in DIII-D advanced plasma scenarios were designed by employing a physics-based model of the

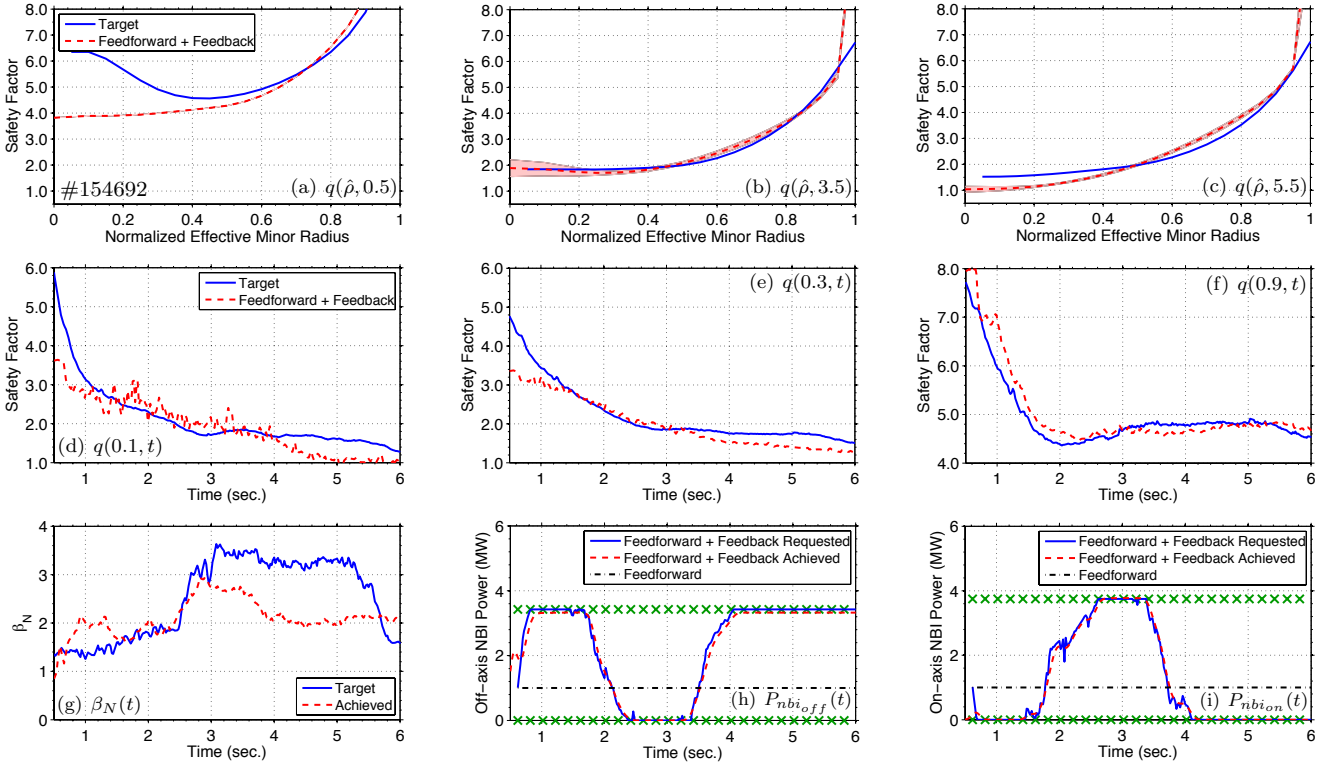

Fig. 6. Experimental testing of q-profile feedback controller during DIII-D shot 154692: (a-c) safety factor profile $q(\hat{\rho})$ at various times, (d-f) time trace of q at various spatial locations, (g) time trace of plasma β_N, and (h-i) control actuator trajectory comparison (actuator limits denoted by green X). Approximate error bars for the experimentally measured q-profiles are shown by the red-shaded regions. Note that the plasma β_N was not feedback-controlled.

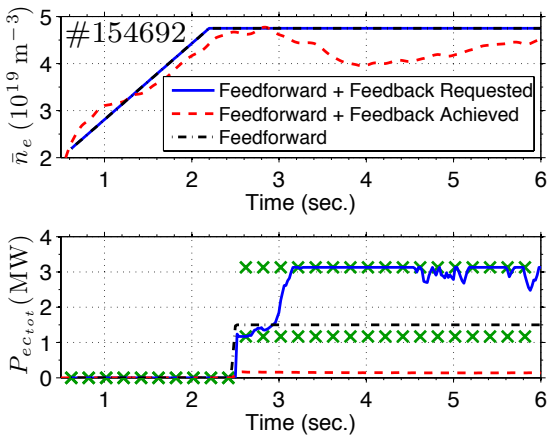

Fig. 7. Line average electron density $\bar{n}_e$ and total gyrotron power $P_{ec_{tot}}$ versus time during DIII-D shot 154692. Actuator limits denoted by green X.

plasma dynamics. The controllers were tested through simulation and experimentally in the DIII-D tokamak. The simulation and experimental results demonstrated the capabilities of the algorithms and provided some insight into the requirements needed to obtain good control performance in advanced scenarios, namely the need to simultaneously achieve a target q-profile and plasma β_N. Our future work includes simultaneously controlling the q-profile and plasma β_N in feedback experiments in DIII-D.

REFERENCES

G. Ambrosino et al. Optimal steady-state control for linear non right-invertible systems. *IET Control Theory and Applications*, 1(3):604–610, 2007.

J. E. Barton, M. D. Boyer, W. Shi, E. Schuster, et al. Toroidal Current Profile Control During Low Confinement Mode Plasma Discharges in DIII-D via First-principles-driven Model-based Robust Control Synthesis. *Nucl. Fusion*, 52:123018, 2012.

J. E. Barton, W. Shi, K. Besseghir, J. Lister, A. Kritz, E. Schuster, et al. Physics-based control-oriented modeling of the safety factor profile dynamics in high performance tokamak plasmas. In *52nd IEEE Conference on Decision and Control*, pages 4182–4187, 2013.

M. D. Boyer, J. E. Barton, E. Schuster, et al. First-principles-driven Model-based Current Profile Control for the DIII-D Tokamak via LQI Optimal Control. *Plasma Phys. Control. Fusion*, 55:105007, 2013.

M. D. Boyer, J. E. Barton, E. Schuster, et al. Backstepping Control of the Toroidal Plasma Current Profile in the DIII-D Tokamak. *IEEE Transactions on Control Systems Technology*, page (in press), 2014.

J. Ferron et al. Real time equilibrium reconstruction for tokamak discharge control. *Nucl. Fusion*, 38:1055, 1998.

F. Hinton and R. Hazeltine. Theory of plasma transport in toroidal confinement systems. *Rev. Mod. Phys.*, 48: 239–308, 1976.

ITER Physics Basis. *Nuclear Fusion*, 39:2137, 1999.

A. Packard. *Whats New with μ: Structured Uncertainty in Multivariable Control.* PhD thesis, Univ. of Calif., Berkeley, 1988.

A. G. Peeters. The bootstrap current and its consequences. *Plasma Phys. and Control. Fusion*, 42:B231–B242, 2000.

S. Skogestad and I. Postlethwaite. *Multivariable Feedback Control Analysis and Design.* Wiley, New York, 2005.

J. Wesson. *Tokamaks.* Oxford, UK: Clarendon Press, 2004.